https://doi.org/10.1016/j.enconman.2018.03.059

Manuscript prepared for Energy Conversion and Management

A general distributed parameter model for ground heat exchangers with arbitrary shape and type of heat sources

Tian You[a,b], Baolong Wang[a], Xianting Li[a,*], Wenxing Shi[a], Hongxing Yang[b]

a Department of Building Science, Beijing Key Lab of Indoor Air Quality Evaluation and Control, School of Architecture, Tsinghua University, Beijing, China

b Renewable Energy Research Group, The Hong Kong Polytechnic University, Hong Kong, China

* Corresponding author: Prof. Xianting Li

Department of Building Science, School of Architecture

Tsinghua University

Beijing 100084, P.R. China

Tel: +86-10-62785860

Fax: +86-10-62773461

E-mail: xtingli@tsinghua.edu.cn

Abstract

The heat and mass transfer simulation model of a ground heat exchanger (GHE) directly affects the design and operation performance of a ground-coupled heat pump system. The GHE models based on the response function (like the Green function and g-function) can achieve a fast calculation speed. However, the heat sources in these models are limited to points or whole boreholes, leading to low calculation accuracy in heat transfer during a short time period and limitation to a certain GHE. A general distributed parameter model for a ground heat exchanger (RF model) is proposed based on the principle of response factors in this paper. A sandbox experimental platform is then built to test the temperatures of typical points in the double-layered soil and to validate the RF model. After that, the calculation of the RF model is simplified by determining suitable positions for the soil boundaries and the numbers of sub pipes and sub soil boundaries. Finally, the RF model is applied in different scenarios to demonstrate its characteristics. The results show that: (1) the RF model is suitable for different kinds of GHEs with arbitrary shape and type of heat sources releasing heat in arbitrary time steps; (2) the RF model has only 0.01 ºC and 0.23 ºC temperature response errors compared to those from numerical solutions and experiments, respectively; (3) the general RF model has similar accuracy to the numerical solution in calculating the distributed temperatures of the borehole and pipes, heat transfer in the short term, and heat transfer of borehole groups and the energy pile.

Keywords: ground-coupled heat pump; ground heat exchanger; distributed parameter model; response factor; simulation

46

47 # Nomenclature

A, B, C	index
c	specific heat capacity, J/(kg·°C)
CON	the current temperature of a point in the soil field influenced by all the previous heat fluxes of heat sources
F	area, m^2
h	heat convection coefficient, W/(m^2·°C)
L	length of U pipe, m
m	mass flow rate, kg/s
Q	heat flux, W
S	area, m^2
V	volume, m^3
Y	response factor
τ	time, s
ρ	density, kg/m^3
λ	heat conductivity, W/(m·°C)

θ	excess temperature, °C
ε	temperature error, °C

48

49 **Subscript**

A	absolute error
k	kth layered soil
n	nth heat source
p	soil point P
r	relative error
s	heat source of heat exchange pipe
w	heat source of soil boundary
$s_s, n_s,$	$n_s,^{th}$ sub heat source of the $s,^{th}$ pipe
$w_w, m_w,$	$m_w,^{th}$ sub heat source of the $w,^{th}$ pipe
f	fluid
pw	pipe wall
in	pipe inlet
out	pipe outlet

50

1 Introduction

The ground-coupled heat pump (GCHP) is becoming more and more popular around the world [1,2] because it is a clean and efficient technology for heating and cooling [3-5]. They are applied not only in the commercial and residential buildings [6, 7], but also in the historical buildings [8] and agricultural facilities [9]. The ground heat exchanger (GHE) is an important component of the GCHP, of which the heat exchanging performance has greatly influenced the system design and operation [10, 11].

There are currently a number of GHE models considering the effect of groundwater, which is beneficial to the heat transfer [12-21]. For example, Hecht-Mendez et al. [15, 16] evaluated different numerical tools and studied the optimized energy extraction for borehole groups considering groundwater. Angelotti et al. [17] adopted MT3DMS coupled to MODFLOW to simulate U pipe in a saturated porous medium. Molina-Giraldo et al. [18] evaluated the effect of thermal dispersion on temperature plumes around a borehole using analytical solutions. Diao et al. [19] proposed an analytical moving line source model to calculate heat transfer with groundwater. Hu [20] and Erol and François [21] improved the analytical model considering both multilayer and groundwater. However, there are also many studies [22-24] aim to predict the heat transfer characteristics of GHE with dry soils, through various analytical and numerical models. On these occasions, the influence of groundwater can be ignored and the heat transfer around the GHE is purely unsteady

heat conduction, thus the calculation models can be simplified. This study focuses on the improvement of the calculation accuracy and speed of the existing GHE models with relatively dry soil or negligible groundwater. In addition, some other important factors should also be considered in the soil field, such as different types and geometries of heat sources, different soil layers and different properties of soil and grout [25-28]. In the existing research, there are three main GHE models: numerical solutions, g-function models and the analytical solutions, which are specifically introduced in the following parts.

Numerical solutions, like the finite difference method [29], finite element method [30-32] and finite volume method [23-24, 33-36], can consider the complex geometries of GHE to calculate the soil temperature distribution accurately. However, since these solutions need to calculate heat and mass transfer of all the meshes in the soil field, they have a heavy workload and are very time-consuming. Especially for cases with different operation strategies, they should repeat similar numerical work on the whole calculation field.

To simplify the calculation, current GHE models commonly use a response function, like the Green function or g-function. These response functions build a direct relation between the temperature and heat sources. Based on them, the heat transfer is no longer calculated in the whole soil field and therefore the calculation time is saved compared with numerical solutions.

The Green function defines a transient point as the heat source [37]. Integrating

93 the Green function over the geometry and the heating time of the sources can achieve
94 the soil temperature. Since the heat source of the Green function is the transient point,
95 the workload is large if it is calculated by numerical simulations [38], and several
96 assumptions should be made if it is calculated by analytical solutions. Analytical
97 solutions [22, 39-44] have a discount on accuracy because of the many assumptions.
98 The commonly used infinite and finite line source models ignore the practical
99 geometry of the borehole, the thermal capacity inside the borehole and the
100 groundwater flow. So, they cause apparent errors in the transient heat transfer and
101 cannot calculate accurately with the variable inlet fluid temperature. Li [43, 44]
102 modified the analytical solution for calculating the short-term heat transfer. However,
103 it ignored the practical geometry of the U pipe and was not suitable for spiral pipes
104 [43] and was unreasonable in the long-term calculation [44].

105 The g-function [45-50] defines a whole borehole with a constant heat flux as the
106 heat source. The borehole here is cylindrical instead of a line source, however the heat
107 transfer inside the borehole is steady in Eskilson model [45], which is reasonable only
108 when the heat source releases heat for longer than 3~12h. Thus, this solution still has a
109 non-negligible error when calculating short-term heat transfer. To improve this model,
110 Yavuzturk et al.[46] and Gallero et al.[47] proposed the short time-step g-function
111 model. This model built a two-dimensional numerical model to describe the unsteady
112 heat transfer inside the borehole, making it suitable for short-term heat transfer.
113 However, this model assumed a fixed heat flux ratio between the inlet and outlet pipe,

ignoring the influence of the fluid velocity.

As a summary, the geometry and type of heat sources of the Green function and g-function in the existing models are limited, leading to inaccurate calculation of the heat transfer of the soil around the GHE. In the research on ventilation, the response factor was used to reflect the relationship between the source and the field [51]. The heat source of the response factor can be an arbitrary shape and releases heat in an arbitrary time-step. This overcomes the limitation of the Green function and g-function, allowing accurate calculation of the heat transfer. In our previous research [52], the definition of the response factors used for soil heat conduction is introduced and the soil temperature distribution influenced by a borehole with a constant heat flux is calculated.

In this paper, based on the principle of the response factor in soil heat conduction, 1) the different types of heat sources in the soil around the GHE are summarized; 2) the calculation methods of the heat fluxes of different heat sources based on the different known parameters are deduced; 3) the general distributed parameter GHE model is proposed to calculate the soil and fluid temperature distribution accurately and fast. So, the unsteady heat transfer outside the pipe, the fluid temperature variation along the flow direction, heat transfer from soil boundaries, rapidly varied fluid temperature and the inner thermal influence between borehole groups can be considered. Then, a sandbox experiment is established to validate the accuracy of the proposed model, and the suitable position of the soil boundaries and the suitable

number of sub heat sources are determined to reduce the calculation workload as well as to guarantee the calculation accuracy. Finally, several cases under different conditions are calculated to show the accuracy of the proposed model in practical projects.

2 The general distributed parameter model for GHE

In the soil, the GHE can be of different types, like boreholes, energy piles with U pipes or spiral pipes, energy walls or energy tunnels. The energy piles/walls/tunnels are geostructures incorporating the primary heat exchangers through the foundation elements (e.g., piles and basement walls) or into the tunnel linings [53]. But for different GHEs, for the pipes buried inside, the inlet temperature and fluid velocity are known, and the fluid temperature varies along the direction of flow. The soil surface has a known temperature which can be considered as similar to the outdoor or indoor air temperature. The surrounding and bottom soil boundaries have a constant initial soil temperature. As a summary, there are two kinds of heat sources in the soil, pipes and the soil boundaries, as shown in Figure 1. Since the heat fluxes of a pipe or a soil boundary are not homogeneous, the pipe or soil boundary should be divided into several small sub heat sources and each sub heat source has a homogeneous heat flux. Each pipe's inlet temperature and fluid velocity are known, and each soil boundary's temperature is known. The correct calculation of heat fluxes of the pipes and soil boundaries will be introduced in the following section 2.3 and its applications

will be shown in section 4.3 and section 5.

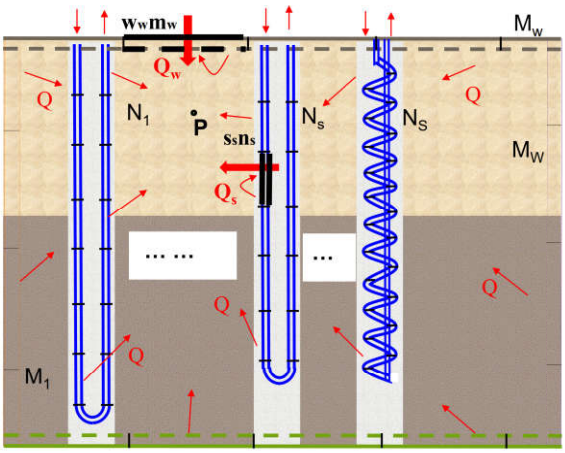

Figure 1 The soil field around the GHE

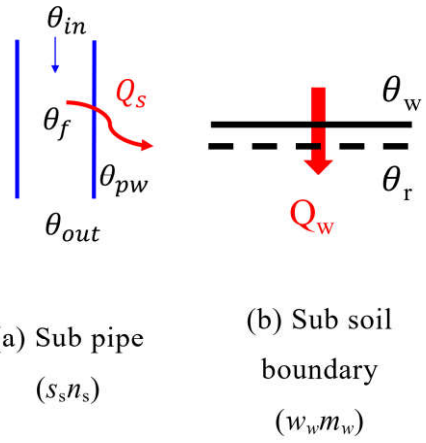

Figure 2 Heat transfer of two kinds of heat sources

The response factor can overcome the limitations of the Green function and g-function on the geometries of the heat sources and the length of the calculation time-steps, reflecting the relationship between the soil temperature variation and the heat flux of a heat source. So, the general distributed parameter model for the GHE is built based on the response factors to calculate the heat transfers in the soil field shown in Figure 1. First, the principle of response factors proposed previously [52] will be introduced briefly. Then, the method for calculating the heat transfer in the soil field based on the response factors and the heat fluxes will be proposed. After that, the calculation of the heat fluxes of the pipes and soil boundaries based on the different known parameters will be deduced. Finally, the distributed soil temperature can be calculated.

2.1 Principle of response factors

In our previous work [52], the principle of response factors in soil heat conduction was proposed. To calculate the response factors, one heat source in any shape releases a heat pulse at the initial time-step of an arbitrary length, while the heat fluxes of all the other heat sources are 0. The excess soil temperature variation affected by the heat pulse is calculated by numerical simulation. The response factor is equal to the excess soil temperature variation divided by the average soil temperature variation caused by the heat pulse at the initial time-step, as shown in Equation (1) [52].

$$Y_{n,p}(j\Delta\tau)=\frac{\theta_p(j\Delta\tau)}{Q_n(0)\cdot\Delta\tau/(\sum_{k=1}^{K}\rho_k c_k V_k)} \tag{1}$$

where $Y_{n,p}(j\Delta\tau)$ is the response factor at the jth time-step of soil point P to the nth heat source; $\theta_p(j\Delta\tau)$ is the excess temperature at the jth time-step of point P after the heat pulse is released by the nth heat source [°C]; $Q_n(0)$ is the heat pulse released by the nth heat source [W]; ρ_k is the density of the kth soil [kg/m^3]; c_k is the specific heat capacity of the kth soil [J/(kg·°C)]; V_k is the volume of the kth soil [m^3].

Therefore, the response factors are dimensionless and tend to be 1 when the time becomes long enough. Although the response factor reflects the relationship between the soil temperature variation and the heat flux, it is an inherent characteristic of the soil field, having no relationship with the heat flux.

Based on the definition of response factors in soil heat conduction, the soil temperature can be calculated by the accumulated contribution of heat fluxes in

different time-steps. The calculation method is shown in Equation (2), which is the accumulation of the heat fluxes multiplied by the corresponding response factors during the period and divided by the soil heat capacity.

$$\theta_p(j\Delta\tau) = \sum_{n=1}^{N}\sum_{i=0}^{j} Q_n(i\Delta\tau)\cdot\Delta\tau\cdot Y_{n,p}[(j-i)\Delta\tau]/(\sum_{k=1}^{K}\rho_k c_k V_k) \quad (2)$$

where $\theta_p(j\Delta\tau)$ is the excess temperature of point P at the j^{th} time-step [°C]; N is the total number of different heat sources.

Since the response factors are based on the results of the numerical simulation, the method based on response factors has similar accuracy to the numerical solutions. Besides, the temperature of several typical soil points can be calculated directly by the heat fluxes and response factors, and calculation of the temperature of surrounding soil points is no longer needed, allowing a fast calculation.

2.2 Heat transfer in soil field around GHE

Based on the response factors of different heat sources at different time-steps, the heat transfer in the soil field should be calculated in the following steps.

Firstly, the numerical model of the soil field around the GHE should be established, considering the specific characteristics of the soil field and GHE (like the complex geometry of the pipes and different thermophysical properties of multi-layered soil, grouts and concretes). The temperature variation of typical soil points influenced by the initial heat pulse of each heat source can be calculated by numerical simulation. Then, the response factors of typical soil points to each heat

source can be calculated based on Equation (1).

$$\theta_p(j\Delta\tau) = CON\theta_{s,p} + CON\theta_{w,p} + \theta_{s,p}(j\Delta\tau) + \theta_{w,p}(j\Delta\tau) \quad (3)$$

After that, taking point P anywhere in the soil as an example, its current temperature can be calculated by Equation (3). This means that the temperature of soil point P at the j^{th} time-step [$\theta_p(j\Delta\tau)$] is the sum of 4 parts: 1) CON$\theta_{s,p}$, the current temperature of P influenced by all the heat fluxes of the pipes in the past time-steps [$Q_s(i\Delta\tau)$ (i=0~(j-1))]; 2) CON$\theta_{w,p}$, the current temperature of P influenced by all the heat fluxes of the soil boundaries in the past time-steps [$Q_w(i\Delta\tau)$ (i=0~(j-1))]; 3) $\theta_{s,p}(j\Delta\tau)$, current temperature of P influenced by all the heat fluxes of the pipes in the current time-step [$Q_s(j\Delta\tau)$]; 4) $\theta_{w,p}(j\Delta\tau)$, the current temperature of P influenced by all the heat fluxes of the soil boundaries in the current time-step [$Q_w(j\Delta\tau)$]. All 4 parts can be calculated by the principle of response factors, as shown in Appendix I.

The response factors of each heat source can be calculated by numerical simulation in advance as the known quantities in Equation (3). As for the heat fluxes, those in the past time-steps [$Q_s(i\Delta\tau)$ and $Q_w(i\Delta\tau)$, (i=0~(j-1))] are known, while those in the current time-step [$Q_s(j\Delta\tau)$ and $Q_w(j\Delta\tau)$] are unknown. Therefore, to calculate the soil temperature at the j^{th} time-step, it is important to calculate the heat fluxes at the j^{th} time-step, including those of the pipes and soil boundaries [$Q_s(j\Delta\tau)$ and $Q_w(j\Delta\tau)$].

2.3 The heat fluxes of pipes and soil boundaries

The calculation of heat fluxes of pipes and soil boundaries is deduced in this

section based on the known parameters. The pipes have known inlet fluid temperatures and fluid velocities. Taking the sub heat source of pipe $s_s n_s$ in Figure 1 as an example, the temperature of the pipe wall is influenced by all the heat sources in the soil field, calculated by Equation (4).

The heat transfer inside the sub pipe is shown in Figure 2(a). The current heat flux of the pipe can be calculated by heat convection between the fluid and the pipe, as shown in Equation (5), in which the heat convection coefficient can be calculated by the empirical equation (Equation (6), [54]) and the definition of Nu number (Equation (7)), and the unknown $\theta_{in}(j\Delta\tau)$, $\theta_{out}((j\Delta\tau)$ and $\theta_{pw}((j\Delta\tau)$ can be calculated by Equation (8)~(9) and Equation (4).

$$\theta_{pw(s_S n_S)}(j\Delta\tau) = CON\theta_{s,\,pw(s_S n_S)} + CON\theta_{w,\,pw(s_S n_S)} + \theta_{s,\,pw(s_S n_S)}(j\Delta\tau) + \theta_{w,\,pw(s_S n_S)}(j\Delta\tau) \tag{4}$$

$$\begin{cases} Q_{S(s_S n_S)}(j\Delta\tau) = h_{f(s_S n_S)} F_{pw(s_S n_S)} \left[\theta_{f(s_S n_S)}(j\Delta\tau) - \theta_{pw(s_S n_S)}(j\Delta\tau) \right] \\ \theta_{f(s_S n_S)}(j\Delta\tau) = \dfrac{\theta_{in(s_S n_S)}(j\Delta\tau) + \theta_{out(s_S n_S)}(j\Delta\tau)}{2} \end{cases} \tag{5}$$

$$\begin{cases} Nu = 0.023 \cdot \mathrm{Re}_f^{0.8} \cdot \mathrm{Pr}_f^{0.3} & \mathrm{Re} > 10000 \\ Nu = 0.116 \cdot (\mathrm{Re}_f^{2/3} - 125) \cdot \mathrm{Pr}_f^{1/3} \cdot (1 + (\dfrac{d_{pipe}}{l_{pipe}})^{2/3} & 2200 < \mathrm{Re} < 10000 \\ Nu = 1.86 \cdot (\mathrm{Re}_f \cdot \mathrm{Pr}_f \cdot \dfrac{d_{pipe}}{l_{pipe}})^{1/3} & \mathrm{Re} < 2200, \mathrm{Pr} > 0.6 \end{cases} \tag{6}$$

$$h_f = \frac{\lambda_f \times Nu}{d_{pipe}} \tag{7}$$

$$\theta_{in(s_S',1)}(j\Delta\tau) = known \qquad (s' = 1,2,\ldots, s, \ldots, S) \tag{8}$$

$$\begin{cases} \theta_{in(s_S n_S)}(j\Delta\tau) = \theta_{in(s_S 1)}(j\Delta\tau) - \sum_{k=1}^{n_S - 1} Q_{S(s_S k)}(j\Delta\tau) / \left(c_{f_S} m_{f_S}\right) \\ \theta_{out(s_S n_S)}(j\Delta\tau) = \theta_{in(s_S 1)}(j\Delta\tau) - \sum_{k=1}^{n_S} Q_{S(s_S k)}(j\Delta\tau) / \left(c_{f_S} m_{f_S}\right) \end{cases} \quad (9)$$

where h_f is the heat convection coefficient of the fluid [W/(m^2·°C)]; λ_f is the heat conductivity of the fluid [W/(m·°C)]; c_{fs} and m_{fs} are the specific heat [J/(kg·°C)] and mass flow rate [kg/s] of fluid inside the pipe of the sth borehole; F_{pw} is the area of the pipe wall [m^2]; $Q(j\Delta\tau)$ is the heat flux of the heat source at the j^{th} time-step [W]; $\theta_f(j\Delta\tau)$ is the average excess fluid temperature inside the pipe at the j^{th} time-step [°C]; $\theta_{pw}(j\Delta\tau)$ is the average excess temperature of the pipe wall [°C]; $\theta_{in}(j\Delta\tau)$ is the average excess inlet temperature of the pipe [°C]; $\theta_{out}(j\Delta\tau)$ is the average excess outlet temperature of the pipe [°C].

Based on Equations (4)~(9), the heat flux of the pipe ($s_s n_s$) is shown in Equation (10). It is the sum of 2 parts: 1) $Q_{s,s(ssns)}(j\Delta\tau)$, the heat flux of the pipe ($s_s n_s$) caused by the heat fluxes of all pipes at all time-steps; and 2) $Q_{w,s(ssns)}(j\Delta\tau)$, heat flux of the pipe ($s_s n_s$) caused by the heat fluxes of all the soil boundaries at all time-steps. In Equation (10), all the current heat fluxes of the pipes and soil boundaries are unknown. In other words, the heat flux of the sub pipe ($s_s n_s$) is the function of the unknown current heat fluxes of all the heat sources in the soil. It is the same case for the other sub pipes. The detailed calculations of Equation (10) are shown in Appendix II.

$$Q_{S(s_S n_S)}(j\Delta\tau) = Q_{s,s(s_S n_S)}(j\Delta\tau) + Q_{w,s(s_S n_S)}(j\Delta\tau) \quad (10)$$

The calculation of the heat fluxes of the soil boundaries is deduced based on the known boundary temperatures. Taking the sub soil boundary $w_w m_w$ as an example, the

heat transfer of the soil boundary is shown in Figure 2(b). Based on the Fourier heat conduction law, the current heat transfer can be calculated by the temperature difference between the soil boundary and its adjacent soil layer, as shown in Equation (11). Since the adjacent layer is in the soil, its temperature is influenced by all the heat sources in the soil field based on the principle of response factors, calculated by Equation (12).

$$Q_{w(w_w m_w)}(j\Delta\tau) = \lambda_{w(w_w m_w)} \frac{F_{w(w_w m_w)}}{\delta_{w(w_w m_w)}} \times \left[\theta_{w(w_w m_w)}(j\Delta\tau) - \theta_{r(w_w m_w)}(j\Delta\tau) \right] \quad (11)$$

$$\theta_{r(w_w m_w)}(j\Delta\tau) = CON\theta_{S,r(w_w m_w)} + CON\theta_{w,r(w_w m_w)} + \theta_{S,r(w_w m_w)}(j\Delta\tau) + \theta_{w,r(w_w m_w)}(j\Delta\tau) \quad (12)$$

Based on Equations (11)~(12), the heat flux of the sub soil boundary ($w_w m_w$) is shown in Equation (13). It is the sum of 2 parts: 1) $Q_{S,w(w_w m_w)}(j\Delta\tau)$ is the heat flux of the sub soil boundary ($w_w m_w$) caused by the heat fluxes of all the pipes at all time-steps; and 2) $Q_{w,w(w_w m_w)}(j\Delta\tau)$ is the heat flux of the sub soil boundary ($w_w m_w$) caused by the heat fluxes of all the soil boundaries at all time-steps. In Equation (13), the current heat fluxes of all the pipes and soil boundaries are unknown. In other words, the heat flux of the sub soil boundary ($w_w m_w$) is the function of the unknown current heat fluxes of all the heat sources in the soil. It is the same case for the other sub soil boundaries. The detailed calculations of Equation (13) are shown in Appendix III.

$$Q_{w(w_w m_w)}(j\Delta\tau) = Q_{S,w(w_w m_w)}(j\Delta\tau) + Q_{w,w(w_w m_w)}(j\Delta\tau) \quad (13)$$

2.4 The distributed soil temperature

Based on Equation (10) and Equation (13), the current heat fluxes of each sub pipe and each sub soil boundary ($Q_s(j\Delta\tau)$ and $Q_w(j\Delta\tau)$, $s=s_1 1, \ldots, s_1 N_1, \ldots\ldots, s_S 1, \ldots, s_S N_S$, $w=w_1 1, \ldots, w_1 M_1, \ldots, w_W 1, \ldots, w_W M_W$) are the function of the current fluxes of all the heat sources ($Q_s(j\Delta\tau)$ and $Q_w(j\Delta\tau)$) in the soil, as is shown in Equation (14). For all the heat sources in the soil around the GHE, both the numbers of heat transfer equations and the unknown current heat fluxes are $N_1+N_2+\ldots+N_S+M_1+M_2+\ldots+M_W$. Therefore, the current heat fluxes of all the heat sources, the inlet and outlet fluid temperatures of each sub pipe, the pipe wall temperature of each sub pipe, and the temperature of the adjacent soil layer of each soil boundary can be calculated based on Equation (14). After the current heat fluxes of all the heat sources are calculated, the typical soil temperatures can be calculated by Equation (3).

$$
\begin{cases}
Q_{s(s_1 1)}(j\Delta\tau) = Q_{s,s(s_1 1)}(j\Delta\tau) + Q_{w,s(s_1 1)}(j\Delta\tau) \\
\ldots \\
Q_{s(s_1 N_1)}(j\Delta\tau) = Q_{s,s(s_1 N_1)}(j\Delta\tau) + Q_{w,s(s_1 N_1)}(j\Delta\tau) \\
\ldots\ldots \\
Q_{s(s_S 1)}(j\Delta\tau) = Q_{s,s(s_S 1)}(j\Delta\tau) + Q_{w,s(s_S 1)}(j\Delta\tau) \\
\ldots \\
Q_{s(s_S N_S)}(j\Delta\tau) = Q_{s,s(s_S N_S)}(j\Delta\tau) + Q_{w,s(s_S N_S)}(j\Delta\tau) \\
\ldots\ldots \\
Q_{w(w_1 1)}(j\Delta\tau) = Q_{s,w(w_1 1)}(j\Delta\tau) + Q_{w,w(w_1 1)}(j\Delta\tau) \\
\ldots \\
Q_{w(w_1 M_1)}(j\Delta\tau) = Q_{s,w(w_1 M_1)}(j\Delta\tau) + Q_{w,w(w_1 M_1)}(j\Delta\tau) \\
\ldots\ldots \\
Q_{w(w_W 1)}(j\Delta\tau) = Q_{s,w(w_W 1)}(j\Delta\tau) + Q_{w,w(w_W 1)}(j\Delta\tau) \\
\ldots \\
Q_{w(w_W M_W)}(j\Delta\tau) = Q_{s,w(w_W M_W)}(j\Delta\tau) + Q_{w,w(w_W M_W)}(j\Delta\tau)
\end{cases}
\tag{14}
$$

3 Validation of the distributed parameter GHE model

Since there are many unknown factors that affect the performance of the GHE in practical projects, the testing errors are usually large and not suitable for verifying the model directly. The sandbox experiment is built with a constant inlet temperature and flow rate of the fluid inside the U pipe. The distributed soil temperatures are tested by the experiment and simulated by numerical solution to validate the RF model.

3.1 The sandbox experiment

The sandbox experiment is composed of a sandbox integrated with thermocouples, a data acquisition system, a water bath providing constant temperature water and a flow meter, as shown in Figure 3 and Figure 4.

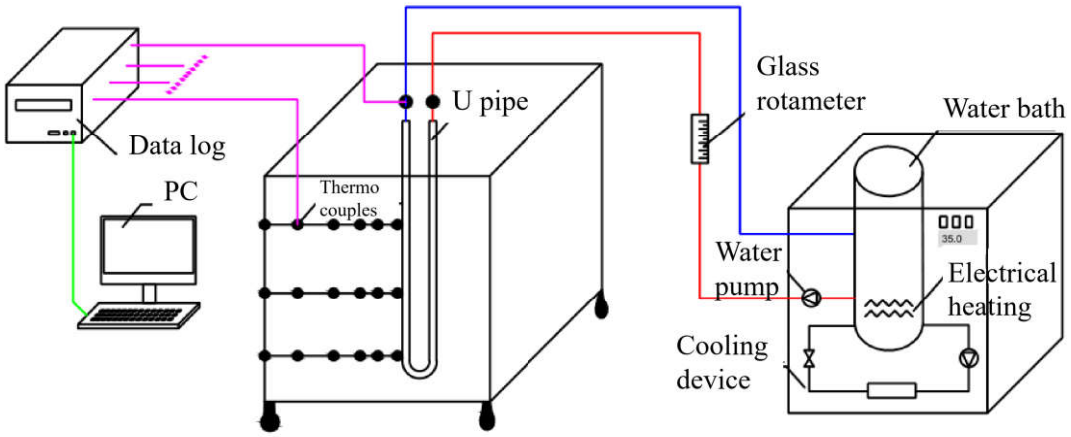

Figure 3 The principle of the sandbox experiment

The sandbox is 1m×1m×1m with a U pipe placed at the center of the sandbox. The inner diameter and length of the U pipe are 8 mm and 950 mm respectively.

There are 6 T-type thermocouples testing the soil temperature at each depth of 250 mm, 500 mm, and 750 mm, as shown in Figure 3. Besides, the indoor air temperature, the constant water temperature of the pool, and the inlet and outlet water temperature of the pipe are tested. A glass rotameter is used to test the flow rate inside the U pipe. The testing range and uncertainty of the sensors are shown in Table 1. The testing range and uncertainty of the glass rotameter are 2~18 LPM and ±0.1 LPM respectively. The testing range and uncertainty of the T-type thermocouples are -150~200 °C and ±0.5 °C respectively. The data log records every 10 seconds.

Figure 4 The sandbox experiment

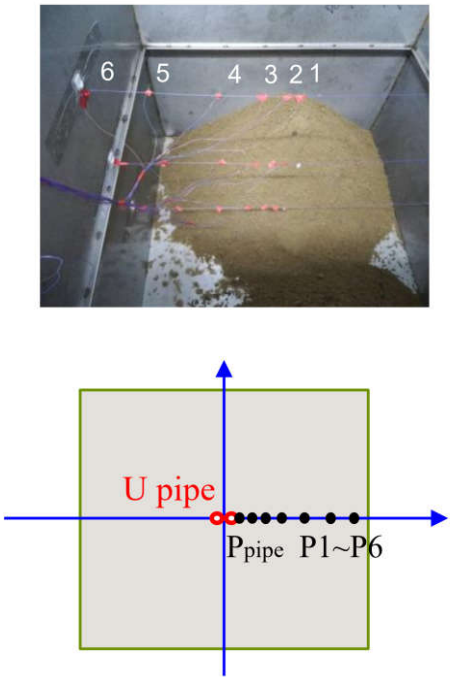

Figure 5 The layout of thermocouples

Table 1 Testing range and uncertainty of the sensors

Sensors	Testing range	Testing uncertainty
T-type thermocouple	-10~40 °C	±0.5 °C

Glass rotameter	2~18 LPM	±0.1 LPM

All the walls, top and bottom of the sandbox are wrapped with thick insulation materials. Test results show that the initial soil temperature is homogeneous at different points inside the sandbox. The temperature difference is within the testing uncertainty of temperature sensors. So, the influence of the ambient air temperature is ignored, and the boundary of the sandbox is regarded adiabatic. The initial excess soil temperature is homogeneous at 0.

For practical projects in cold regions (like Shenyang), the initial soil temperature could be 11°C and the inlet temperature could be 1°C. So, the excess inlet temperature of the U pipe remains constant at about -10°C and the water flows inside the U pipe at a flow rate of 3.8 LPM.

To verify the RF model calculating the multi-layered soil, the sandbox is filled with sand at a depth of 430~1000 mm and clay at a depth of 0~430 mm. The soil thermal properties are tested by the cutting-ring method, drying method, and the transient hot-wire method [55-57]. Using these methods, the testing results show that the densities of the sand and clay are respectively 1.26 g/cm^3 and 1.20 g/cm^3, and the thermal diffusivities of the sand and clay are respectively 0.24 mm^2/s and 1.40 mm^2/s.

3.2 Validation of the experiment data

Taking the 6 thermocouples at the depth of 250 mm, for example (Figure 5), their temperatures in 24 hours are tested in the sandbox experiment as well as being calculated by the RF model, and the numerical solution (finite volume method). The

soil temperature variation is shown in Figure 6, in which the different colors or line types mean different thermocouples. The thermocouple next to the U pipe is affected quickly by the U pipe, so its temperature decreases rapidly to the lowest value. The thermocouple far from the U pipe is affected slowly by the U pipe, so its temperature decreases gently.

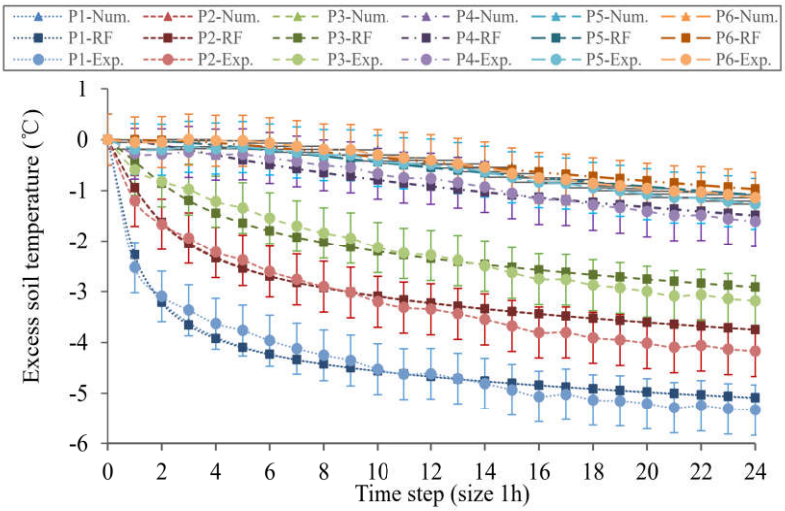

Figure 6 The soil temperature contrast of numerical solution, RF model and experiment

In Figure 6, each color or line type includes three different lines, standing for the results of the same thermocouple from the experiment, RF model, and the numerical solution. The results of the RF model and the numerical solution nearly overlap, between which the average errors are less than 0.01 ºC. The results of the RF model and the experiment are also very similar, between which the average errors are less than 0.23 ºC. Therefore, the RF model is well verified by the numerical solution and validated by the experiment.

4 Simplification of the distributed parameter GHE model

As mentioned in section 2, there are two kinds of heat sources in the soil around the GHE, the pipes and soil boundaries. In the RF model, they are divided into several

sub heat sources to accurately calculate the variable heat fluxes along the flow path inside the pipes and around the soil boundaries. With the number of sub heat sources increasing, the calculation accuracy increases, while the calculation workload also increases.

In addition, the position of the soil boundary also affects the calculation accuracy and workload. If the volume of the soil field around the pipe in the numerical simulation is assumed to be small, the calculation results are unreasonable. If the volume of the soil field around the pipe is assumed to be big, the calculation workload is heavy.

Therefore, in this section, suitable numbers of sub heat sources of pipes and soil boundaries and reasonable positions of the soil boundaries are investigated to achieve good accuracy as well as a small workload.

4.1 The position of soil boundary

Taking the single borehole (depth 100 m, diameter 130 mm, single U pipe) as an example, when the initial soil temperature is 11 °C, the inlet fluid temperature and the velocity of the pipe are respectively constant at 35 °C and 0.4 m/s, the reasonable side and bottom boundaries of the soil field around the GHE in 30 operation years are analyzed. In this simulation, the heat conductivities of the soil, grout and pipe are respectively 1.74, 2.50 and 0.42 W/(m·K).

Ideally, the soil field around a single borehole should be semi-infinite. To reduce the calculation workload, if the excess temperature variations of the soil points are less than 0.5 °C, they are regarded as unaffected by the U pipe. The unaffected side position closest to the GHE is defined as the reasonable side boundary of the soil field

around the GHE. It can reduce the calculation load at the premise of acceptable calculation accuracy. Ignoring the influence of groundwater, the side and bottom boundaries of the soil field around GHE in 30 operation years are shown in Figure 7. With the operation time increasing, the soil boundary should be farther from the U pipe and the bottom of the borehole.

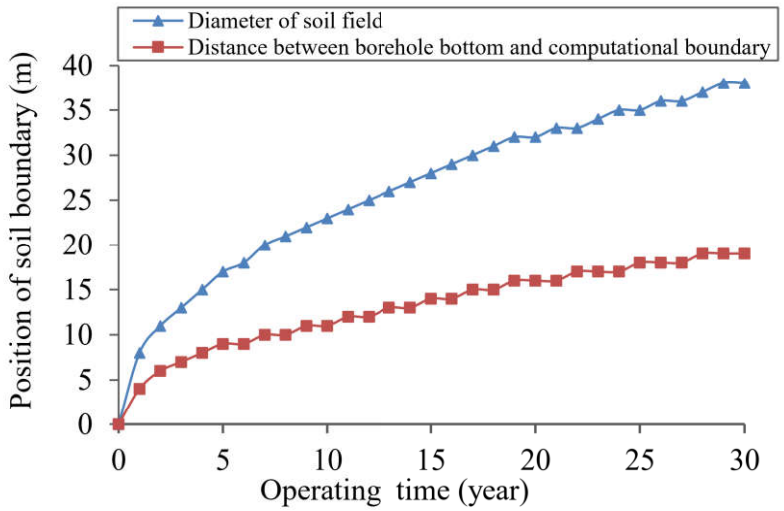

Figure 7 The suggested boundary of the soil field around a single borehole

In China, the lifespans of most GHEs are shorter than 30 years. Based on Figure 7, the position of the soil boundary around a single borehole should be as shown in Figure 8(a). The side soil boundary should be 40 m away from the U pipe and the bottom soil boundary should be 20 m lower than the bottom of the borehole. The temperatures of the side and bottom soil boundaries are constant and equal to the initial soil temperature. The temperature of the soil surface is equal to the variable outdoor air temperature.

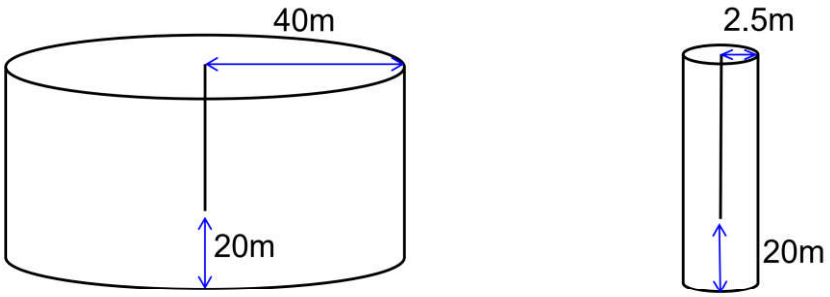

(a) Soil field around a single borehole (b) Soil field around a borehole in a group

Figure 8 The suitable position of the boundary of the soil field

For one borehole in the borehole groups, since the heat flux of each borehole is the same, the side soil boundary of each borehole is adiabatic. The soil field around the borehole is shown in Figure 8(b). The diameter of the soil cylinder is 2.5 m, half of the borehole spacing (typically 5 m [58]).

Taking one borehole in a borehole group as an example, the simplification of sub heat sources of a borehole will be analyzed in section 4.2 and section 4.3. There are three heat sources in the soil field: the U pipe, the soil surface and the bottom soil boundary. The bottom soil boundary has a constant initial soil temperature and its heat transfer variation has less effect on the pipe and soil temperature. So, the bottom soil boundary can be regarded as a single heat source, with no divisions. Due to the variable heat fluxes of the U pipe and the soil surface, these two heat sources should be divided into several sub heat sources and each sub heat source should have a constant heat flux.

4.2 The sub heat sources of pipe

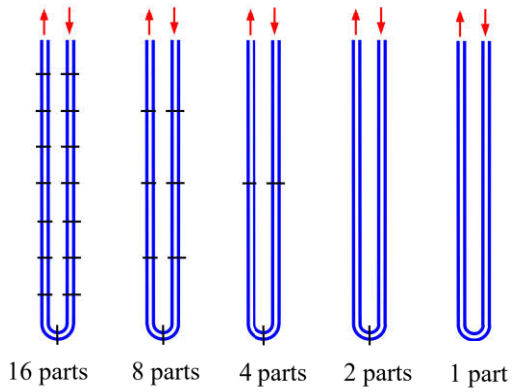

Figure 9 Different sub heat sources of U pipe

To analyze the influence of the number of sub heat sources of the U pipe on the accuracy, the U pipe is divided into several different (16, 8, 4, 2, and 1) sub heat sources, as shown in Figure 9. Their influence on the accuracy in calculating the temperature of the pipe wall, borehole wall and the outlet fluid temperature of the pipe is investigated. The heat conductivities of grout and soil are respectively 2.50 and 1.74 W/(m·K).

The distributed temperature of the U pipe wall, distributed borehole temperature, and outlet fluid temperature are calculated by the RF model (with different sub heat sources of the pipe) over a period of 2880 hours (a typical length of heating season in cold region of China). The average errors of these temperatures calculated by the RF model compared with the numerical solution are based on Equation 15 and shown in Table 2. When the number of sub heat sources of the U pipe increases, the results calculated by the RF model tend to be closer to the numerical solution.

$$\varepsilon_A = \frac{\int_0^L \theta \, ds - (\theta_1 \times l_1 + \ldots + \theta_n \times l_n)}{L} \tag{15a}$$

$$\varepsilon_r = \frac{\int_0^L \theta \, ds - (\theta_1 \times l_1 + ... + \theta_n \times l_n)}{\int_0^L \theta \, ds} \tag{15b}$$

where ε_A is the absolute average error of temperature, °C; ε_r is the relative error of temperature; θ is the distributed excess temperature calculated by numerical simulation, °C; n is n^{th} sub pipe; θ_n is the excess temperature of the n^{th} sub pipe calculated by RF model, °C; l_n is the length of the n^{th} sub pipe, m; L is the length of the whole U pipe, m.

If the number of sub heat sources of the U pipe is 16, the average absolute errors of the results calculated by the RF model are less than 0.110 °C and the relative errors are less than 0.30%. If the number of sub heat sources of the U pipe is more than 2, the average absolute errors calculated by the RF model are less than 0.610 °C and the relative errors are less than 1.48%, which are acceptable in practical projects.

Table 2 Errors of distributed temperatures of pipe wall in the 2880^{th} hour by RF model

	Average errors	**16 parts**	**8 parts**	**4 parts**	**2 parts**	**1 part**
Distributed pipe wall temperature	Absolute values (°C)	0.100	0.160	0.300	0.610	1.380
	Relative values	0.25%	0.40%	0.73%	1.48%	3.34%
Distributed borehole temperature	Absolute values (°C)	0.110	0.320	0.340	0.350	0.650
	Relative values	0.30%	0.87%	0.94%	0.97%	1.78%
Outlet fluid temperature	Absolute values (°C)	0.019	0.012	0.003	0.053	0.262
	Relative values	0.10%	0.07%	0.01%	0.29%	1.43%

As a result, the pipe can be divided into 2~4 sub heat sources, keeping the errors of the pipe wall temperature, borehole wall temperature and the outlet fluid temperature of the U pipe small and acceptable in the practical projects.

4.3 The sub heat sources of soil surface

Although the soil surface has constant temperature at different positions, its heat flux is not homogeneous at different positions influenced by the borehole. So, the soil surface should be divided into different sub heat sources to reflect the different heat fluxes. To analyze the influence of the number of sub heat sources of the soil surface on the accuracy, the soil surface is divided into several different (8, 4, 2, and 1) sub heat sources, as shown in Figure 10. Their influence on the accuracies in calculating the temperature of the pipe wall, the outlet fluid temperature of the pipe and the temperature of the soil layer adjacent to the soil surface is investigated.

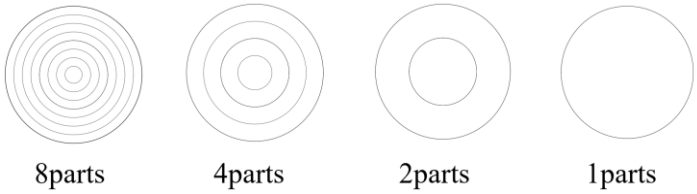

Figure 10 Different sub heat sources of soil surface

The distributed excess temperatures of the U pipe wall and excess temperature of the pipe outlet calculated by the RF model (with different sub heat sources of soil surface) and the numerical solution are shown in Figure 11. The number of sub heat sources of the soil surface has little influence on the wall temperature and the outlet fluid temperature of the U pipe. The results calculated by the RF model with different sub heat sources of the soil surface are nearly the same.

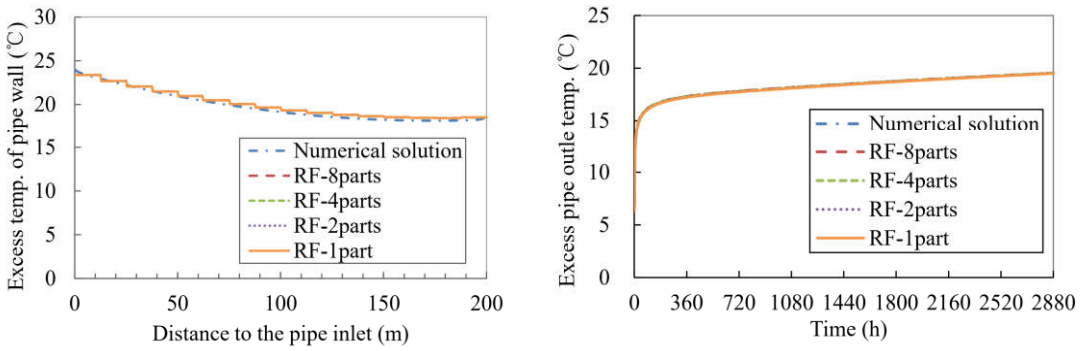

(a) Distributed excess temperature of pipe wall

(b) Excess temperature of pipe outlet

444 Figure 11 Temperatures influenced by sub heat sources of soil boundary

445 The average errors of the temperature of the soil layer adjacent to the soil surface
446 calculated by the RF model (with different sub heat sources of the soil surface)
447 compared with those of the numerical solution in the 2880th hour are based on
448 Equation 16 and are shown in Table 3. Although the temperature of the soil surface is
449 as high as 38 °C, the influence of the different numbers of sub heat sources on its
450 adjacent soil layer is small and there is even less influence on the other parts of the
451 soil. The average errors of the temperature of the adjacent soil layer calculated by the
452 RF model are about 0.0745~0.0751 °C. Consequently, the soil surface can be
453 considered as the whole part.

$$\varepsilon'_A = \frac{\int_0^S \theta \, ds - (\theta_1 \times S_1 + ... + \theta_n \times S_n)}{S} \tag{16}$$

454 where ε'_A is the absolute average error of soil layer temperature, °C; θ is the
455 distributed excess temperature of the adjacent soil layer calculated by numerical
456 simulation, °C; n is nth sub soil surface; θ_n is the excess temperature of the adjacent

457 soil layer of the n^{th} sub soil surface calculated by RF model, °C; S_n is the area of the
458 n^{th} sub soil surface, m^2; S is the area of the whole soil surface, m^2.

459 Table 3 Average errors of the temperature of the adjacent soil layer by the RF model

Average error	8 parts	4 parts	2 parts	1 part
Absolute value (°C)	0.0745	0.0749	0.0749	0.0751

460 # 5 Application of the distributed parameter model

461 In the previous work [52], the calculation based on the principle of response
462 factors was proved to be fast compared with numerical solutions. Besides, the general
463 RF model proposed in this paper also has good accuracies in wide applications by
464 considering complex factors: 1) three-dimensional unsteady heat transfer inside the
465 borehole; and 2) practical geometries of the GHE, like borehole groups with different
466 depths and different GHE structures. So, it can calculate 1) the distributed temperature
467 inside the borehole and pipes, 2) the heat transfer of the borehole in the short term and
468 under variable conditions, 3) the heat transfer of borehole groups with different depths,
469 and even 4) the heat transfer around the energy pile.

470 ## 5.1 The distributed temperature along the U pipe and borehole depth

471 The RF model can consider the practical three-dimensional heat transfer inside
472 the borehole. Through the calculation, the temperature variation along the borehole
473 depth and short circuit of the heat transfer of the U pipe are investigated in this
474 section.

475 Taking a 100 m borehole with a single U pipe as an example, the distributed
476 temperatures along the borehole depth and U pipe are calculated by the RF model.

The borehole and the U pipe are divided into 8 and 16 sub parts respectively, as shown in Figure 12. The initial soil temperature is 11 °C, which is the annual mean soil temperature of Shenyang, a city in cold region of China. If there is no measured data, the soil temperature could be typically regarded as 1~3°C higher than the annual average air temperature [59]. The weather file is from the Chinese Architecture-specific Meteorological Data Sets for Thermal Environment Analysis [60]. The inlet fluid temperature is 35 °C and the soil surface temperature is 38 °C. The temperatures of different sub parts of the borehole at the 1st hour, 24th hour, 240th hour, 1000th hour and 2880th hour are shown in Figure 13, calculated by the RF model, the numerical solution, and the analytical solution. The results from the RF model are similar to the numerical solution, which demonstrates that the temperature of sub parts of the borehole drops as its depth increases. As a contrast, the borehole temperature calculated by the analytical solution using a finite line source remains constant at different depths, because it uses the average borehole temperature for calculation.

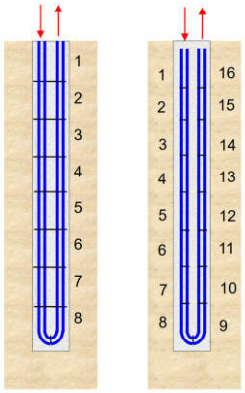

(a) Borehole (b) U pipe

Figure 12 The sub parts of the borehole and U pipe

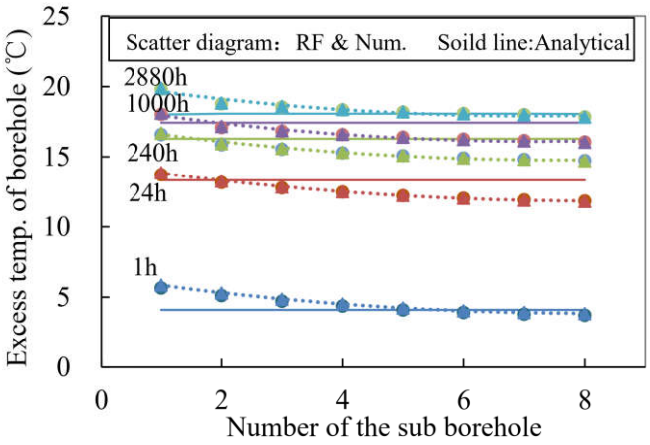

Figure 13 The temperature variation along the borehole depth at different times

The distributed temperature and heat transfer of the U pipe wall calculated by the RF model are shown in Figure 14. The temperature of the sub pipe wall drops seriously along the flow direction for the sub pipes near the inlet and has a tiny increase in the sub pipes near the outlet. The heat transfer of the No. 16 sub pipe is negative, showing the short circuit of the heat transfer between the two legs of the U pipe near the soil surface.

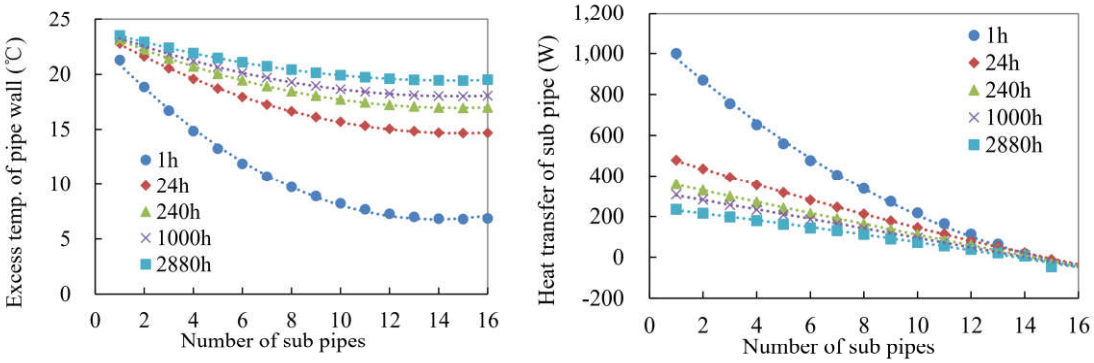

(a) Distributed temperature (b) Heat transfer

Figure 14 The distributed temperature and heat transfer of U pipe wall

5.2 The heat transfer in a short term and under variable conditions

As mentioned in the introduction, most analytical solutions cannot calculate accurately for the heat transfer in a short term (usually less than a couple of hours). The RF model can improve the calculation accuracy on this issue because it considers the three-dimensional unsteady heat transfer inside the borehole. Since the numerical solution can consider the detailed characteristics of the GHE, it is considered to be the most accurate method, and the reference for other methods. In this section, the heat transfers in a short term and under variable conditions calculated by the analytical solution (finite line source), RF model, and numerical solution (finite volume method) are compared.

Taking a single U pipe with a length of 100 m as an example, provided the inlet fluid temperature of the U pipe keeps constant at 35.0 ºC and the velocity is 0.4 m/s, the outlet fluid temperature of the U pipe during 50 hours is shown in Figure 15(a). Since the results of the numerical solutions can be accurate in short-term calculation by considering the practical geometry and the grout's thermal property of the borehole, they are considered as the benchmark for the analytical solution and RF model. The errors of the outlet fluid temperature calculated by the analytical solution and RF model compared with the numerical solution are shown in Figure 15(b). From Figure 15, the RF model has a very similar result to the numerical solution, of which the error is less than 0.2 ºC in the initial 50 hours. However, the error of the analytical solution is higher than 3.0 ºC in the first 2 hours. Although it decreases with increasing time, it is still higher than 0.7 ºC in the initial 50 hours.

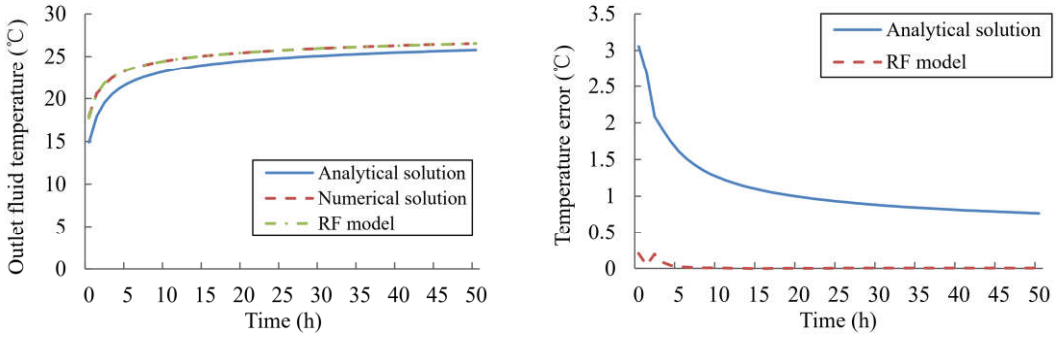

(a) Outlet fluid temperature calculated by the three solutions

(b) Errors of analytical solution and RF model

Figure 15 Outlet fluid temperature and errors in short term

If the calculation error is large in the short term, the method cannot calculate accurately in the case with a variable inlet temperature, leading to shortcomings in the calculation of practical projects.

In a case with a variable inlet temperature of the pipe (calculated by the GCHP system simulation in advance, Figure 16(a)), the outlet temperatures of the pipe calculated by the analytical solution, RF model, and numerical solution, and the errors of the analytical solution and the RF model compared with the numerical solution are shown in Figure 16(b). The result of the RF model is similar to that of the numerical solution, and its error is less than 0.1 ºC all the time. However, the analytical solution has a large error, especially when the inlet temperature of the pipe varies seriously, and its largest transient error is about 0.6 ºC. Therefore, the RF model has a good accuracy in calculating the case with a variable inlet temperature.

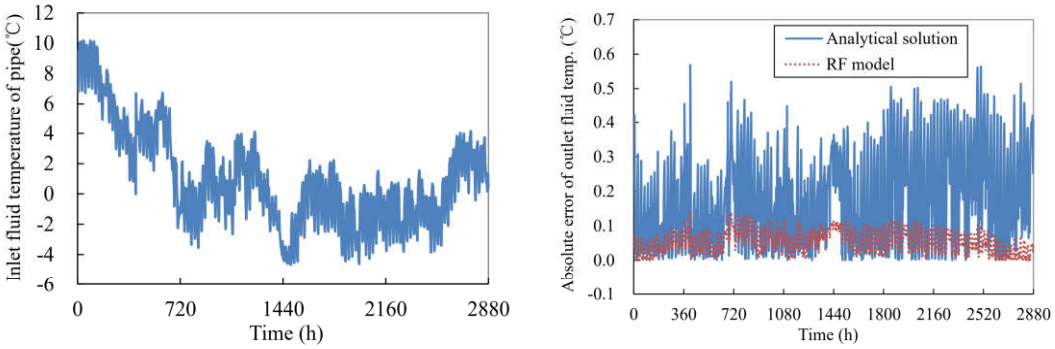

(a) Variable inlet temperature (b) Absolute errors of outlet temperature

Figure 16 Fluid temperature and errors under variable conditions

5.3 Heat transfer of borehole groups with different depths

Due to bad construction quality, some boreholes may have different depths. Can the borehole group provide enough energy in total when the total length of boreholes keeps the same? The RF model is used for the analysis of borehole groups with different depths because it can be used for GHEs with different geometries. Three boreholes with different depths of 80 m, 100 m, and 120 m respectively are shown in Figure 17. Based on the RF model, when the inlet fluid temperature for each borehole

is 24.0 ºC, the outlet fluid temperatures of different boreholes are shown in Figure 18, and are respectively 19.9 ºC, 19.1 ºC, and 18.2 ºC at the 2880th hour. The heat transfers of the boreholes with depths of 80 m, 100 m, and 120 m are 42.42 W/m, 40.36 W/m, and 39.90 W/m respectively.

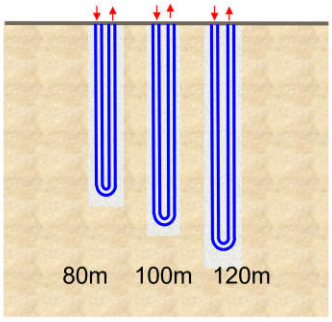

Figure 17 Borehole groups with different depths

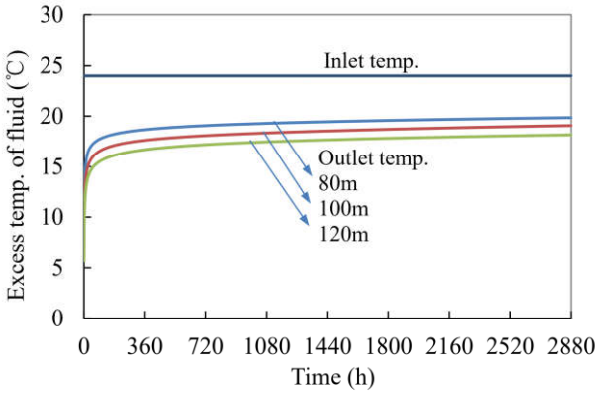

Figure 18 Outlet fluid temperature of pipes in different boreholes

When the total depths of the boreholes groups are the same, the heat transfer of the boreholes with different depths (Figure 17) is compared to that of three boreholes with the same depths of 100 m. Although the heat transfer of each borehole is not the same, the total heat transfers of the borehole groups are the same in the two cases.

5.4 Heat transfer around energy pile

Since the RF model uses the sub pipes as the heat sources, it can be used for different GHE structures, like the energy pile in Figure 19. The finite line source model of the analytical solutions is no longer suitable for the energy pile due to the pile's large diameter. The depth and diameter of the energy pile are 24 m and 1.5 m, and the pipe has three U loops. The temperatures of several points at the cross-section with a depth of 12 m are calculated. The radii of points P1~P6 in concrete are

557 respectively 0, 0.25 m, 0.45 m, 0.55 m, 0.60 m, and 0.67 m. The radii of points
558 P7~P11 are respectively 0.75 m, 0.85 m, 1.50 m, 2.00 m, and 4.00 m.

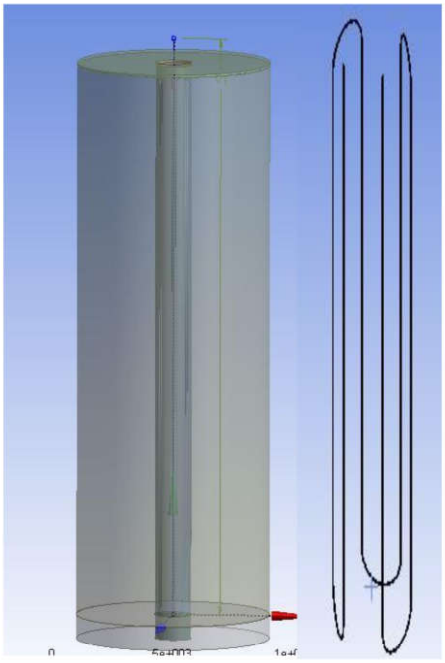

Figure 19 An energy pile with a three-loop pipe inside

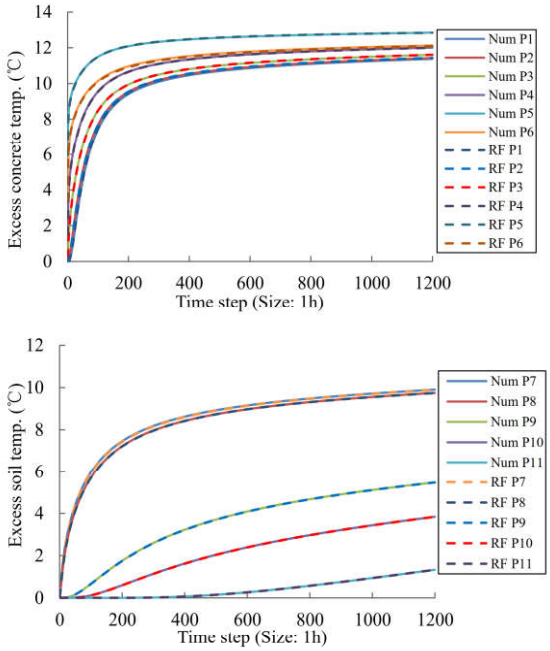

Figure 20 Typical temperature in concrete and soil

559 The typical temperatures of concrete and soil calculated by the RF model and the
560 numerical solution are shown in Figure 20. The results by the RF model are similar to
561 that of the numerical solution, showing the good accuracy of the RF model in
562 calculating an energy pile.

563 6 Conclusions

564 In this paper, the general distributed parameter ground heat exchanger model (RF
565 model) is proposed based on the principle of response factors, calculating the soil
566 temperature and the fluid temperature inside the pipe. By dividing the pipe and the
567 soil boundaries into several small sub heat sources, the general RF model can

568 calculate the soil temperature considering different soil boundaries, three-dimensional
569 unsteady heat transfer inside the borehole, different geometries and structures of the
570 GHE, as well as arbitrary time-steps.

571 A sandbox experiment is conducted to validate the RF model and the simplified
572 method is investigated to reduce the calculation workload of the RF model. Compared
573 to the sandbox experiment and the numerical solution, the average errors of the RF
574 model are less than 0.23 ºC and 0.01 ºC, respectively. Compared to the numerical
575 solution, the number of sub heat sources of each pipe could be as few as 2~4 and the
576 number of sub heat sources of each soil boundary could be 1.

577 Several cases have demonstrated the accuracy of the RF model in different
578 applications: 1) the distributed temperature inside the borehole and pipes, 2) heat
579 transfer of the borehole in a short term and under variable conditions, 3) heat transfer
580 of borehole groups with different depths, and even 4) heat transfer around energy
581 piles.

582 ## Acknowledgments

583 The authors gratefully acknowledge the support of Innovative Research Groups
584 of the National Natural Science Foundation of China (Grant No.51521005) and
585 National Natural Science Foundation of China (Grant No.51638010).

586

Appendix I: Terms in Equation (3)

$$CON\theta_{s,p}=\sum_{i=0}^{j-1}\sum_{s'=1}^{S}\sum_{n_{s'}=1}^{N_{s'}}\left[Q_{s(s_{s'},n_{s'})}(i\Delta\tau)\cdot\Delta\tau\cdot Y_{s(s_{s'},n_{s'}),p}[(j-i)\Delta\tau]/\Sigma_{k=1}^{K}\rho_k c_k V_k\right] \quad (3\text{-a})$$

$$CON\theta_{w,p}=\sum_{i=0}^{j-1}\sum_{w'=1}^{W}\sum_{m_{w'}=1}^{M_{w'}}\left[Q_{w(w_{w'},m_{w'})}(i\Delta\tau)\cdot\Delta\tau\cdot Y_{w(w_{w'},m_{w'}),p}[(j-i)\Delta\tau]/\Sigma_{k=1}^{K}\rho_k c_k V_k\right] \quad (3\text{-b})$$

$$\theta_{s,p}(j\Delta\tau)=\sum_{s'=1}^{S}\sum_{n_{s'}=1}^{N_{s'}}\left[Q_{s(s_{s'},n_{s'})}(j\Delta\tau)\cdot\Delta\tau\cdot Y_{s(s_{s'},n_{s'}),p}(0)/\Sigma_{k=1}^{K}\rho_k c_k V_k\right] \quad (3\text{-c})$$

$$\theta_{w,p}(j\Delta\tau)=\sum_{w'=1}^{W}\sum_{m_{w'}=1}^{M_{w'}}\left[Q_{w(w_{w'},m_{w'})}(j\Delta\tau)\cdot\Delta\tau\cdot Y_{w(w_{w'},m_{w'}),p}(0)/\Sigma_{k=1}^{K}\rho_k c_k V_k\right] \quad (3\text{-d})$$

where Q is the heat flux of a heat source, [W]; subscripts s, w denote the heat source of the pipe and soil boundary respectively; $s_{s'}n_{s'}$ is the $n_{s'}$th sub heat source of the s'th pipe (there are S pipes in the soil field, s'=1, 2,…, s ,…, S; each pipe has $N_{s'}$ parts, N_s=N_1, N_2,…, N_s ,…, N_S); $w_{w'}m_{w'}$ is the $m_{w'}$th sub heat source of the w'th pipe (there are W soil boundaries in the soil field, w'=1,2,…, w ,…,W; each soil boundary has $M_{w'}$ parts, M_w=M_1, M_2,…, M_w, …, M_W); $Y_{s(s_{s'},n_{s'}),p}[(j-i)\Delta\tau]$ is the response factor of soil point (P) to the heat source ($s_{s'}n_{s'}$) at the (j-i)th time-step; $Y_{w(w_{w'},m_{w'}),p}[(j-i)\Delta\tau]$ is the response factor of soil point (P) to the heat source ($w_{w'}m_{w'}$) at the (j-i)th time-step.

Appendix II: Terms in Equation (10)

Classifying the known and unknown parameters in Equations (4)~(9), two terms

in Equation (10) are expressed as Equations (10-a) and (10-b), in which A, B and C are coefficients composed of the known quantities, $Q_s(j\Delta\tau)$ and $Q_w(j\Delta\tau)$ are unknown heat fluxes. The expressions of A, B and C are Equations (10-c) ~ (10-g).

$$Q_{S,s(s_S n_S)}(j\Delta\tau) = A_{S,s(s_S n_S)} - C_{s(s_S n_S)} \cdot \left[\sum_{k=1}^{n_S - 1} Q_{s(s_S k)}(j\Delta\tau) + \frac{1}{2} Q_{s(s_S n_S)}(j\Delta\tau) \right] - \sum_{s'=1}^{S} \sum_{n_{S'}=1}^{N_{S'}} \left[B_{s(s_S, n_S'), pw(s_S n_S)} \cdot Q_{s(s_S, n_S')}(j\Delta\tau) \right] \quad \text{(10-a)}$$

$$Q_{w,s(s_S n_S)}(j\Delta\tau) = A_{w,s(s_S n_S)} - \sum_{w'=1}^{W} \sum_{m_{W'}=1}^{M_{W'}} \left[B_{w(w_W, m_W'), pw(s_S n_S)} \cdot Q_{w(w_W, m_W')}(j\Delta\tau) \right] \quad \text{(10-b)}$$

$$A_{S,s(s_S n_S)} = h_{f(s_S n_S)} F_{pw(s_S n_S)} \times \left\{ \theta_{in(s_S 1)}(j\Delta\tau) - \sum_{i=0}^{j-1} \sum_{s'=1}^{S} \sum_{n_{S'}=1}^{N_{S'}} \left\{ Q_{s(s_S, n_S')}(i\Delta\tau) \cdot \Delta\tau \cdot Y_{s(s_S, n_S'), pw(s_S n_S)}[(j-i)\Delta\tau] / \Sigma_{k=1}^{K} \rho_k c_k V_k \right\} \right\} \quad \text{(10-c)}$$

$$A_{w,s(s_S n_S)} = -h_{f(s_S n_S)} F_{pw(s_S n_S)} \times \left\{ \sum_{i=0}^{j-1} \sum_{w'=1}^{W} \sum_{m_{W'}=1}^{M_{W'}} \left\{ Q_{w(w_W, m_W')}(i\Delta\tau) \cdot \Delta\tau \cdot Y_{w(w_W, m_W'), pw(s_S n_S)}[(j-i)\Delta\tau] / \Sigma_{k=1}^{K} \rho_k c_k V_k \right\} \right\} \quad \text{(10-d)}$$

$$B_{s(s_S, n_S'), pw(s_S n_S)} = h_{f(s_S n_S)} F_{pw(s_S n_S)} \cdot \Delta\tau \cdot Y_{s(s_S, n_S'), pw(s_S n_S)}(0) / \Sigma_{k=1}^{K} \rho_k c_k V_k \quad \text{(10-e)}$$

$$B_{w(w_W, m_W'), pw(s_S n_S)} = h_{f(s_S n_S)} F_{pw(s_S n_S)} \cdot \Delta\tau \cdot Y_{w(w_W, m_W'), pw(s_S n_S)}(0) / \Sigma_{k=1}^{K} \rho_k c_k V_k \quad \text{(10-f)}$$

$$C_{s(s_S n_S)} = \frac{h_{f(s_S n_S)} F_{pw(s_S n_S)}}{\left(c_{f_S} m_{f_S} \right)} \quad \text{(10-g)}$$

Appendix III: Terms in Equation (13)

Classifying the known and unknown parameters in Equations (11)~(12), two terms in Equation (13) are expressed as Equations (13-a) and (13-b), in which A, B and C are coefficients composed of the known quantities, $Q_s(j\Delta\tau)$ and $Q_w(j\Delta\tau)$ are unknown heat fluxes. The expressions of A, B and C are Equations (13-c) ~ (13-f).

$$Q_{S,w(w_W m_W)}(j\Delta\tau) = A_{S,w(w_W m_W)}(j\Delta\tau) - \sum_{s'=1}^{S}\sum_{n_S'=1}^{N_S'}\left[B_{S(s_S,n_S'),w(w_W m_W)} \cdot Q_{S(s_S,n_S')}(j\Delta\tau)\right] \quad (13\text{-a})$$

$$Q_{W,w(w_W m_W)}(j\Delta\tau) = A_{W,w(w_W m_W)}(j\Delta\tau) - \sum_{w'=1}^{W}\sum_{m_W'=1}^{M_W'}\left[B_{W(w_W,m_W'),w(w_W m_W)} \cdot Q_{W(w_W,m_W')}(j\Delta\tau)\right] \quad (13\text{-b})$$

$$A_{S,w(w_W m_W)}(j\Delta\tau) = -\lambda_{w(w_W m_W)}\frac{F_{w(w_W m_W)}}{\delta_{w(w_W m_W)}} \times \sum_{i=0}^{j-1}\sum_{s'=1}^{S}\sum_{n_S'=1}^{N_S'}\left\{Q_{S(s_S,n_S')}(i\Delta\tau)\cdot\Delta\tau\cdot Y_{S(s_S,n_S'),r(w_W m_W)}[(j-i)\Delta\tau]/\Sigma_{k=1}^{K}\rho_k c_k V_k\right\} \quad (13\text{-c})$$

$$A_{W,w(w_W m_W)}(j\Delta\tau) = \lambda_{w(w_W m_W)}\frac{F_{w(w_W m_W)}}{\delta_{w(w_W m_W)}} \times \left\{\theta_{w(w_W m_W)}(j\Delta\tau) - \sum_{i=0}^{j-1}\sum_{w'=1}^{W}\sum_{m_W'=1}^{M_W'}\left\{Q_{W(w_W,m_W')}(i\Delta\tau)\cdot\Delta\tau\cdot Y_{W(w_W,m_W'),r(w_W m_W)}[(j-i)\Delta\tau]/\Sigma_{k=1}^{K}\rho_k c_k V_k\right\}\right\} \quad (13\text{-d})$$

$$B_{S(s_S,n_S'),w(w_W m_W)} = \lambda_{w(w_W m_W)}\frac{F_{w(w_W m_W)}}{\delta_{w(w_W m_W)}}\cdot\Delta\tau\cdot Y_{S(s_S,n_S'),r(w_W m_W)}(0)/\Sigma_{k=1}^{K}\rho_k c_k V_k \quad (13\text{-e})$$

$$B_{W(w_W,m_W'),w(w_W m_W)} = \lambda_{w(w_W m_W)}\frac{F_{w(w_W m_W)}}{\delta_{w(w_W m_W)}}\cdot\Delta\tau\cdot Y_{W(w_W,m_W'),r(w_W m_W)}(0)/\Sigma_{k=1}^{K}\rho_k c_k V_k \quad (13\text{-f})$$

Reference

[1] Chua K, Chou S, Yang W. Advances in heat pump systems: A review. Applied energy, 2010, 87(12): 3611-3624.

[2] Lund J, Freeston D, Boyd T. Direct utilization of geothermal energy 2010 worldwide review. Geothermics, 2011, 40(3): 159-180.

[3] Morrone B, Coppola G, Raucci V. Energy and economic savings using geothermal heat pumps in different climates. Energy Conversion and Management, 2014, 88: 189-198.

[4] Lucia U, Simonetti M, Chiesa G, Grisolia G. Ground-source pump system for heating and cooling: Review and thermodynamic approach. Renewable and Sustainable Energy Reviews, 2017, 70: 867–874.

622 [5] Sarbu I, Sebarchievici C. General review of ground-source heat pump systems
623 for heating and cooling of buildings. Energy and buildings, 2014, 70: 441-454.
624 [6] Zarrella A, Emmi G, De Carli M. A simulation-based analysis of variable flow
625 pumping in ground source heat pump systems with different types of borehole
626 heat exchangers: a case study, Energy Conversion and Management, 2017, 131:
627 135-150.
628 [7] Aira R, Fernández-Seara J, Diz R, Pardiñas Á. Experimental analysis of a
629 ground source heat pump in a residential installation after two years in operation,
630 Renewable Energy, 2017, 114: 1214-1223.
631 [8] Emmi G, Zarrella A, Carli M, Moretto S, Galgaro A, Cultrera M, Tuccio Maria,
632 Bernardi A. Ground source heat pump systems in historical buildings: two
633 Italian case studies, Energy Procedia, 2017, 133: 183-194.
634 [9] Alberti L, Antelmi M, Angelotti A, Formentin G. Geothermal heat pumps for
635 sustainable farm climatization and field irrigation, Agricultural Water
636 Management, 2018, 195: 187-200.
637 [10] Wu W, You T, Wang B, Shi W, Li X. Evaluation of ground source absorption
638 heat pumps combined with borehole free cooling. Energy Conversion and
639 Management, 2014, 79: 334-343.
640 [11] Yang H, Cui P, Fang Z. Vertical-borehole ground-coupled heat pumps: a review
641 of models and systems. Applied Energy, 2010, 87(1), 16-27.
642 [12] Jahangir M, Sarrafha H, Kasaeian A. Numerical Modeling of Energy Transfer in

643 Underground Borehole Heat Exchanger within Unsaturated Soil, Applied
644 Thermal Engineering, 2018, 132: 697-707.
645 [13] Piga B, Casasso A, Pace F, Godio A, Sethi R. Thermal Impact Assessment of
646 Groundwater Heat Pumps (GWHPs): Rigorous vs. Simplified Models, Energies,
647 2017, 10(9): 1385.
648 [14] Casasso A, Sethi R. Efficiency of closed loop geothermal heat pumps: A
649 sensitivity analysis, Renewable Energy, 2014, 62: 737-746.
650 [15] Hecht‐Méndez J, Molina‐Giraldo N, Blum P, Bayer P. Evaluating MT3DMS
651 for heat transport simulation of closed geothermal systems, Groundwater, 2010,
652 48(5): 741-756.
653 [16] Hecht-Méndez J, Paly De M, Beck M, Bayer P. Optimization of energy
654 extraction for vertical closed-loop geothermal systems considering groundwater
655 flow, Energy conversion and management, 2013, 66: 1-10.
656 [17] Angelotti A, Alberti L, La Licata I, Antelmi M. Borehole Heat Exchangers: heat
657 transfer simulation in the presence of a groundwater flow, Journal of Physics:
658 Conference Series. IOP Publishing, 2014, 501(1): 012-033.
659 [18] Molina-Giraldo N, Bayer P, Blum P. Evaluating the influence of thermal
660 dispersion on temperature plumes from geothermal systems using analytical
661 solutions, International Journal of Thermal Sciences, 2011, 50(7): 1223-1231.
662 [19] Diao N, Li Q, Fang Z. Heat transfer in ground heat exchangers with
663 groundwater advection, International Journal of Thermal Sciences, 2004, 43(12):

664 1203-1211.

665 [20] Hu J. An improved analytical model for vertical borehole ground heat
666 exchanger with multiple-layer substrates and groundwater flow, Applied Energy,
667 2017, 202: 537-549.

668 [21] Erol S, François B. Multilayer analytical model for vertical ground heat
669 exchanger with groundwater flow, Geothermics, 2018, 71: 294-305.

670 [22] Dehghan B, Kukrer E. A new 1D analytical model for investigating the long
671 term heat transfer rate of a borehole ground heat exchanger by Green's function
672 method, Renewable Energy, 2017, 108: 615-621.

673 [23] Li X, Li T, Qu D, Yu J. A new solution for thermal interference of vertical
674 U-tube ground heat exchanger for cold area in China, Geothermics, 2017, 65:
675 72-80.

676 [24] Choi H, Yoo G, Pak J, Lee C. Numerical study on heat transfer characteristics in
677 branch tube type ground heat exchanger, Renewable Energy, 2018, 115:
678 585-599.

679 [25] Alberti L, Angelotti A, Antelmi M, La Licata I. A Numerical Study on the
680 Impact of Grouting Material on Borehole Heat Exchangers Performance in
681 Aquifers, Energies, 2017, 10(5): 703.

682 [26] Delaleux F, Py X, Olives R, Dominguez A. Enhancement of geothermal
683 borehole heat exchangers performances by improvement of bentonite grouts
684 conductivity, Applied Thermal Engineering, 2012, 33: 92-99.

685 [27] Erol S, François B. Freeze damage of grouting materials for borehole heat
686 exchanger: Experimental and analytical evaluations, Geomechanics for Energy
687 and the Environment, 2016, 5: 29-41.
688 [28] Lee C, Lee K, Choi H, Choi H. Characteristics of thermally-enhanced bentonite
689 grouts for geothermal heat exchanger in South Korea, Science in China Series E:
690 Technological Sciences, 2010, 53(1): 123-128.
691 [29] Rottmayer S, Beckman W, Mitchell J. Simulation of a single vertical Utube
692 ground heat exchanger in an infinite medium. ASHRAE Transactions, 1997;
693 103(2): 651–9.
694 [30] Gultekin A, Aydin M, Sisman A. Thermal performance analysis of multiple
695 borehole heat exchangers. Energy Conversion and Management, 2016, 122:
696 544-551.
697 [31] Yoon S, Lee S, Go G. A numerical and experimental approach to the estimation
698 of borehole thermal resistance in ground heat exchangers. Energy, 2014, 71:
699 547–555.
700 [32] Pärisch P, Mercker O, Oberdorfer P, Bertram E, Tepe R, Rockendorf G.
701 Short-term experiments with borehole heat exchangers and model validation in
702 TRNSYS. Renewable Energy, 2015, 74: 471–477.
703 [33] Wang Z, Wang F, Liu J, Ma Z, Han E, Song M. Field test and numerical
704 investigation on the heat transfer characteristics and optimal design of the heat
705 exchangers of a deep borehole ground source heat pump system. Energy

706 Conversion and Management, 2017, 153: 603-615.

707 [34] Dai L, Shang Y, Li X, Li S. Analysis on the transient heat transfer process inside
708 and outside the borehole for a vertical U-tube ground heat exchanger under
709 short-term heat storage. Renewable Energy, 2016, 87: 1121-1129.

710 [35] Wang J, Long E, Qin W. Numerical simulation of ground heat exchangers based
711 on dynamic thermal boundary conditions in solid zone. Applied Thermal
712 Engineering, 2013, 59(1–2): 106–115.

713 [36] Pu L, Qi D, Li K, Tan H, Li Y. Simulation study on the thermal performance of
714 vertical U-tube heat exchangers for ground source heat pump system. Applied
715 Thermal Engineering, 2015, 79: 202–213.

716 [37] Jia L, FangZ. Advanced heat transfer theory, second version, Beijing: Higher
717 Education Press, 2008. (in Chinese)

718 [38] Wang B, Jiang Y. The eigenvalue method for analysing on unstable heat transfer
719 during a long time. Journal of Engineering Thermophysics, 1984, 03: 284-287.
720 (in Chinese)

721 [39] Ingersoll L, Plass H. Theory of the ground pipe heat source for the heat pump.
722 ASHVE Transactions, 1948, 54: 339-348.

723 [40] Zeng H, Diao N, Fang Z. A finite line-source model for boreholes in geothermal
724 heat exchangers. Heat Transfer Asian Research, 2002, 31(7): 558–567.

725 [41] Koohi-Fayegh S, Rosen M. An analytical approach to evaluating the effect of
726 thermal interaction of geothermal heat exchangers on ground heat pump

727 efficiency. Energy Conversion and Management, 2014, 78: 184-192.

728 [42] Minaei A, Maerefat M. A new analytical model for short-term borehole heat
729 exchanger based on thermal resistance capacity model, Energy and Buildings,
730 2017, 146: 233-242.

731 [43] Li M, Lai A. Analytical solution to heat conduction in finite hollow composite
732 cylinders with a general boundary condition. International Journal of Heat and
733 Mass Transfer, 2013, 60: 549–556.

734 [44] Li M, Lai A. Analytical model for short-time responses of ground heat
735 exchangers with U-shaped tubes: model development and validation. Applied
736 Energy, 2013, 104: 510-516.

737 [45] Eskilson P. Thermal analysis of heat extraction boreholes[Doctoral thesis]. Lund,
738 Sweden: University of Lund, 1987.

739 [46] Yavuzturk C, Spitler J. A short time step response factor model for vertical
740 ground loop heat exchangers. ASHRAE Transactions, 1999, 105: 475–485.

741 [47] Gallero F, Maestre I, Gómez P, Blázquez J. Numerical and experimental
742 validation of a new hybrid model for vertical ground heat exchangers. Energy
743 Conversion and Management, 2015, 103: 511-518.

744 [48] Lamarche L. g-function generation using a piecewise-linear profile applied to
745 ground heat exchangers, International Journal of Heat and Mass Transfer, 2017,
746 115: 354-360.

747 [49] M. Cimmino, M. Bernier. A semi-analytical method to generate g-functions for

748 geothermal bore fields, International Journal of Heat Mass Transfer, 2014, 70:
749 641–650.
750 [50] Dusseault B, Pasquier P, Marcotte D. A block matrix formulation for efficient
751 g-function construction, Renewable Energy, 2017.
752 [51] Zhu F, Investigation on dynamic state distribution of indoor contaminant in
753 ventilated room/system with recirculation[Master thesis]. Beijing: China:
754 Tsinghua University, 2009. (in Chinese)
755 [52] You T, Shi W, Wang B, Wang H, Li X. A fast distributed parameter model of
756 ground heat exchanger based on response factor. Building Simulation, 2016,
757 1-10.
758 [53] Rees S, Advances in Ground-Source Heat Pump Systems. Woodhead Publishing,
759 2016.
760 [54] Diao N, Fang Z. Ground-coupled heat pump technology, Beijing: High
761 education Press, 2006. (in Chinese)
762 [55] Cui S, Zhang H, Zhang M. Swelling characteristics of compacted GMZ
763 bentonite–sand mixtures as a buffer/backfill material in China. Engineering
764 geology, 2012, 141: 65-73.
765 [56] Assael M, Antoniadis K, Metaxa I, Mylona S, Assael J, Wu J, Hu M. A Novel
766 Portable Absolute Transient Hot-Wire Instrument for the Measurement of the
767 Thermal Conductivity of Solids, International Journal of Thermophysics, 2015,
768 36(10-11): 3083-3105.

769 [57] Li H, Liu Z, Xu Z, Wang D, Shi L. Development of virtual simulation
770 experiment for thermal conductivity and thermal diffusivity by using plane heat
771 source method, Experimental Technology and Management,
772 2017,34(05):5-7+10. (in Chinese)
773 [58] Ministry of Construction in the People's Republic of China.
774 GB50366-2005(2009 version). Code for engineering technologies in groud
775 source heat pump system, Beijing: China Architecture and Building Press, 2009.
776 (in Chinese)
777 [59] Wu W, Wang B, You T, Shi W, Li X. A potential solution for thermal imbalance
778 of ground source heat pump systems in cold regions: ground source absorption
779 heat pump. Renewable energy, 2013, 59: 39-48.
780 [60] Department of Building Science of Tsinghua University. Chinese architecture
781 specific meteorological data sets for thermal environment analysis. Beijing:
782 China Architecture and Building Press; 2005. (in Chinese)